AIAA JOURNAL
Vol. 51, No. 7, July 2013

Flameholding in Converging and Turning Channels over Cavities with Periodic Port Injection

Ben J. Colcord,* William A. Sirignano,† and Feng Liu‡
University of California, Irvine, California 92697-3975

DOI: 10.2514/1.J051890

The deliberate continuation of the combustion in the turbine passages of a gas-turbine engine has the potential to increase the efficiency and the specific thrust or power of current gas-turbine engines. This concept, known as a turbine burner, introduces certain challenges concerning the injection, mixing, ignition, and burning of fuel within a short residence time in a turbine passage characterized by large three-dimensional accelerations. Here, the injection of the fuel into a cavity adjacent to the modeled turbine passage is examined, which creates a low-speed zone for mixing and flameholding. The turbine passage is modeled as a converging and curving channel flow of high-temperature vitiated air adjacent to a cavity. To give a broader understanding of the cavity channel-flow coupling, both constant-area and converging channels with both straight and curving centerlines are modeled. Three-dimensional unsteady calculations with periodic port injection are performed, examining the effects of channel convergence and curvature, and injection configurations. These direct simulations address flows with Reynolds-number values up to 2000. Calculations show that converging channels reduce the combustion efficiency. Channel curvature can be either beneficial or detrimental to combustion efficiency, depending on the location of the cavity, and the fuel- and air-injection configuration. Injecting fuel and air so as to disrupt the natural rotation of the fluid in the cavity stimulates three-dimensional instability and improves the combustion efficiency.

Nomenclature

A	=	preexponential reaction constant
a_c	=	centrifugal acceleration, m/s^2
a, b	=	chemical rate exponents
D	=	cavity depth, m
$\mathcal{D}$	=	diffusion coefficient, m^2/s
E	=	total energy per unit mass, J/kg
E_a	=	activation energy, J/kg
Fr	=	Froude number
H	=	stagnation enthalpy, J/kg
h	=	enthalpy, J/kg
k	=	thermal conductivity, W/m · K
L	=	injector half-width, m
l	=	cavity length, m
M	=	Mach number, mixedness
$\dot{m}$	=	mass flow rate, kg/s
p	=	pressure, N/m^2
Q_F	=	heat of reaction for fuel, J/kg
R	=	centerline radius, m
R_u	=	universal gas constant, J/kg · K
Re	=	Reynolds number
r	=	radial coordinate, m
T	=	temperature, K
T_c	=	calculation time, s
t	=	time, s
U	=	freestream velocity, m/s
u, v, w	=	local velocity, m/s
V	=	volume, m^3
x, y, z	=	Cartesian coordinates, m
Y_m	=	mass fraction of species m
y_m	=	modified mass fraction of element m

Greek symbols

α	=	mixedness normalizing variable
δ_{ij}	=	Kronecker delta
η_c	=	combustion efficiency
μ	=	dynamic viscosity, kg/m · s
ρ	=	density, kg/m^3
τ_{ij}	=	stress tensor, kg/m · s^2
τ_r	=	residence time, s
Φ	=	Rayleigh discriminant, rad^2/s^2
ϕ	=	equivalence ratio
Ω	=	angular velocity, rad/s
$\dot{\omega}$	=	chemical reaction rate, kg/m^3 · s

Subscripts

C	=	carbon atom
F	=	fuel
i, j	=	directional index
in	=	inflow
m	=	index for chemical species
N	=	nitrogen atom
p	=	perfectly mixed
∞	=	freestream condition

I. Introduction

THERMODYNAMIC analyses by Sirignano and Liu [1] show that purposely adding heat in the turbine of a gas-turbine engine has the potential to reduce the afterburner length and weight, and/or reduce the specific fuel consumption compared with turbojets with afterburners. Compared with turbojets without afterburners, the turbine burner has the potential to increase the specific thrust. In a similar analysis for ground-based gas-turbine engines, the turbine burner shows an increase in both specific power and thermal efficiency. From these analyses, it is concluded that, contrary to the historical view that it should be avoided, augmented burning in the turbine passages offers an opportunity to improve the performance of gas-turbine engines. This concept is known as a turbine burner. A comprehensive review of the current turbine-burner research has been presented by Sirignano et al. [2].

Received 9 February 2012; revision received 26 December 2012; accepted for publication 5 February 2013; published online 23 May 2013.

*Graduate Student Researcher, Department of Mechanical and Aerospace Engineering. Member AIAA.

†Professor, Department of Mechanical and Aerospace Engineering. Fellow AIAA.

‡Professor, Department of Mechanical and Aerospace Engineering. Fellow AIAA.

Liu and Sirignano [3] extended the concept of the turbine burner to include, not only the continuous burning in the turbine, but also configurations, in which the turbine stators double as combustors, effectively introducing discrete interstage turbine burners. The continuous turbine burner (CTB) and the interstage turbine burner with M stages (M-ITB) were compared with conventional turbojet and turbofan engines in a thermodynamic analysis. Both the CTB and the M-ITB show significantly higher specific thrust with no or only small increases in the thrust specific fuel consumption. The turbine-burner engines also perform consistently well across a wide range of flight Mach numbers and compressor pressure ratios, whereas the performance of the conventional engine declines rapidly outside of its operational range. The performance gain of turbine-burner engines over conventional engines increases with increasing compressor pressure ratio, fan bypass ratio, and/or flight Mach number.

The turbine passages are characterized by transonic unsteady flows with very large three-dimensional (3-D) accelerations. Combined with the relatively short length of the turbine passages, transonic-flow speeds mean that the mixing, ignition, and burning of the fuel are required in a very short residence time. Additionally, the incoming flow from the combustor is a mixture of burned and unburned gases with significant spatial variations in temperature, composition, and density, which cause further complications.

Acceleration in the streamwise direction through the turbine passages can reach the order of 10^5 g, but, because of the transverse density gradient, the actual value of the streamwise acceleration will vary substantially in the transverse direction. This variation in turn creates large transverse velocity gradients or highly strained flows. Strained flows can enhance mixing and heat transfer because of increased interface areas, but the variations in local velocity can also create variations in residence times for different flow paths. This can produce further flammability difficulties, in which the residence times are shorter. One method of increasing the residence time of the flow is to use a cavity to create a low-speed zone where fuel and any additional air can be injected so that it has sufficient time for mixing and combustion to occur.

There is a substantial literature addressing the use of cavities for flameholding, most of it inspired by scramjet technology or compact combustors for gas-turbine-engine applications. Hsu et al. [4,5] considered gaseous propane and air injected into an axisymmetric cavity to achieve low-speed flame stabilization. They showed that a vortex is locked in a short cavity with $l/d < 1$ and stable flames resulted for cavity lengths between 0.45 and 0.65 of the upstream wall diameter. Longer cavities produced unstable flames, whereas shorter cavities lacked enough volume for flameholding. Similar results showing a limited l/d range for a stable flame zone were obtained by Katta and Roquemore [6,7] from time-dependent computational fluid dynamics calculations, also with gaseous propane as the fuel.

Studies at the Wright–Patterson Air Force Research Laboratories examined the effectiveness of cavities for flame stabilization in high-speed flows. Numerical simulations [8–10] of nonreacting cavity flows showed that cavity residence times decreased in longer cavities and cavities with slanted downstream walls. These studies showed that, for cavities of fixed length, the residence time is approximately proportional to the depth, whereas the residence time decreases with increased cavity length for cavities of fixed depth. Therefore, the length of the cavity determines the mass exchange rate between the channel and the cavity, whereas the cavity depth determines the residence time. Additionally, Davis and Bowersox [9,10] used their results to obtain an empirical equation for the required depth of the cavity: $d = \tau_r U_\infty/40$. Yu et al. studied the influence of the cavity geometry on the combustion of ethylene [11] and kerosene [12–15] fuel injected upstream of the cavity in a Mach 2 flow. They showed that small-aspect-ratio cavities provide better flameholding than longer cavities. They also combined a short open cavity with a downstream closed cavity, which was demonstrated to have a higher combustion efficiency than a single open cavity. Numerical studies by Kim et al. [16] showed that increasing the wall angle of the downstream cavity wall increased the combustion efficiency, but also increased the total pressure loss. Combustion efficiency and total pressure loss were both shown to increase with the cavity length-to-depth ratio in the range $l/d = 2$–4.

Rasmussen et al. [17] have studied the effects of a cavity on stability limits in supersonic flow. They showed that injecting fuel from the downstream wall or ramp gave better performance near the lean blowout limit, whereas injecting from the floor of the cavity gave more stable flames near the rich limit. They also showed that between Mach 2 and Mach 3, the lean blowout limit did not change significantly, whereas the Mach number had a measurable effect near the rich limit.

Our work here focuses on the coupling between the cavity flow and the flow in the simulated turbine-stator passage with flameholding as one major goal. This goal differs from the aforementioned works, which aim at flameholding in scramjets or in compact combustors external to a turbine stage. The turbine passages in a gas-turbine engine are characterized by large accelerations both in the streamwise and transverse directions due to the convergence and turning of the turbine blades. Also, it is only desirable to add enough fuel in the cavity/turbine stator to burn some, but not all, of the vitiated air entering the passage, that is, we still have a temperature-limited situation. Furthermore, the best strategy for combustion in the turbine nozzle vane is to have it begin in the upstream portion where the Mach number is lower. Nevertheless, the effects of turning and streamwise acceleration are important and are examined in our analysis.

We have a few previous works on this turbine burner. For example, Puranam et al. [18] performed experiments with propane injection into a cavity in a curved converging channel. They found that there are three distinct regimes for combustion, depending on the air-mass flow rates. At low air flow rates, the combustion is confined to the shear layer downstream of the cavity. At high air flow rates, combustion occurred almost exclusively in the cavity. At moderate flow rates, the flame was not stable in the cavity, and fluctuated between burning in the shear layer and in the cavity. Puranam et al. [18], using the same type of cavity/channel configuration to the kind studied here (but a different injection scheme), achieved experimentally the desired enthalpy increase for a turbine burner.

Flow acceleration has been considered in flows without cavities. Sirignano and Kim [19] derived similarity solutions for a laminar two-dimensional (2-D) mixing layer for both reacting and nonreacting flows with axial acceleration. They assumed that the chemical kinetic rate was very fast and the reaction zone was very thin. These similarity solutions offer some insight into the effect of flow acceleration on the flame structure in the mixing layer. It was shown that the mixing layer remains very thin for accelerating flow and that the peak temperature was found to decrease with downstream distance. These results imply that the NO_x formation would be less than that which occurs in a flow without acceleration. A mixing and exothermic chemical reaction in the accelerating flow through the turbine passage offers, therefore, an opportunity for a major technological improvement in both performance and pollutant mitigation. The reduction in peak temperatures due to acceleration results in the promise of reduced pollutant formation and reduced heat-transfer losses in other combustion applications as well.

Fang et al. [20] extended that study to mixing layers with arbitrary pressure gradients and finite rate chemical kinetics by using a finite difference method for the boundary-layer equations. The influence of pressure gradients, initial temperature, initial pressure, initial velocity, and transport properties was studied. Mehring et al. [21] performed a numerical study on a reacting, turbulent, and accelerating mixing layer. Cai et al. [22] developed a finite volume method for solving the 2-D compressible Favre-averaged Navier–Stokes equations with chemical reactions using the Baldwin–Lomax turbulence model. Cheng et al. [23–25] showed that, for accelerating transonic mixing layers, the shear-layer instability for accelerating flows had smaller fluctuation compared to nonaccelerating flows.

The Kelvin–Helmholtz instability occurs in most cavity flows due to the velocity shear at the upstream lip. In 2-D and 3-D flows, turning channels introduce two new modes of instability: the Rayleigh–Taylor instability and the Rayleigh centrifugal instability. A third instability is introduced in 3-D flows: the Görtler instability [26]. The Rayleigh–Taylor instability occurs when a force acts in the direction

of a density gradient. This situation is unstable if the density decreases in the direction of the force. The Rayleigh centrifugal instability occurs due to the dynamical effects of rotation or of streamline curvature. A necessary and sufficient condition for centrifugal stability is that $\Phi \geq 0$ everywhere, in which Φ is the Rayleigh discriminant defined by

$$\Phi(r) = \frac{1}{r^3}\frac{\mathrm{d}}{\mathrm{d}r}(r^2\Omega)^2 \tag{1}$$

The Görtler instability occurs in flows along concave surfaces, and manifests as vortical structures with axes parallel to the flow. Therefore, the Görtler instability is a 3-D phenomenon.

Colcord et al. [27] performed 2-D numerical simulations of fuel injection into cavities in turning and converging channels. This work showed that converging channels improve the combustion efficiency by improving the mixing.

The current work models a simplified turbine burner as a converging, turning channel flow over a cavity. The calculations are 3-D with symmetry-plane boundary conditions in the spanwise direction. The injection ports, therefore, represent an infinite periodic array of injectors. We have not extended channel convergence to the extent that transonic flow is reached; we do, however, have some calculations, in which sufficiently high subsonic velocities are reached and compressibility becomes important.

Section II presents the numerical models used. Section III gives the results of the numerical calculations for reacting flows in straight channels (Sec. III.A), converging channels (Sec. III.B), turning channels (Sec. III.C), and turning and converging channels (Sec. III.D). Finally, Sec. IV gives our conclusions.

II. Analysis and Numerical Modeling

The computational domain is a 3-D curved channel over a cavity. The compressible Navier–Stokes equations are solved, together with energy and species equations:

$$\frac{\partial \rho}{\partial t} + \frac{\partial \rho u_j}{\partial x_j} = 0 \tag{2}$$

$$\frac{\partial \rho u_i}{\partial t} + \frac{\partial \rho u_j u_i}{\partial x_j} = -\frac{\partial p}{\partial x_i} + \frac{\partial \tau_{ij}}{\partial x_j} \tag{3}$$

$$\frac{\partial \rho E}{\partial t} + \frac{\partial \rho u_j H}{\partial x_j} = \frac{\partial}{\partial x_j}\left(k\frac{\partial T}{\partial x_j}\right) + \frac{\partial}{\partial x_j}(u_i\tau_{ij}) + Q_F\dot{\omega}_F \tag{4}$$

$$\frac{\partial \rho Y_m}{\partial t} + \frac{\partial \rho u_j Y_m}{\partial x_j} = \frac{\partial}{\partial x_j}\left(\mathcal{D}\frac{\partial Y_m}{\partial x_j}\right) + \dot{\omega}_m \tag{5}$$

in which

$$\tau_{ij} = \mu\left(\frac{\partial u_i}{\partial x_j} + \frac{\partial u_j}{\partial x_i}\right) - \frac{2}{3}\mu\delta_{ij}\frac{\partial u_j}{\partial x_j} \tag{6}$$

$$E = H - \frac{p}{\rho} \tag{7}$$

$$H = h + \frac{1}{2}(u^2 + v^2 + w^2) \tag{8}$$

Uniform constant velocity, temperature, and species mass fraction are prescribed at the inlet, and pressure is uniformly fixed at the exit. Zero-gradient conditions are applied, in which values are not prescribed. Walls are adiabatic, with slip allowed only on the wall opposite the cavity. Boundaries in the z direction are symmetry planes. The exit pressure is 1 atm, and the inlet conditions are $T = 1000$ K and vitiated mixture of 50% combustion products and 50% air. Density is calculated assuming a perfect gas, and the inlet velocity is varied to give the desired Reynolds number. All calculations are performed using OpenFOAM [28], an open-source C++ package. The reactingFoam solver is used with additional modifications. This solver uses the PISO algorithm for pressure coupling. The time discretization is second-order implicit backward differencing with a prescribed maximum Courant–Friedrichs–Lewy number of 0.5. Gaussian integration is used for the spatial discretization, with linear interpolation from cell centers to cell faces for second-order derivatives and the Sweby flux limiter [29] for first-order derivatives. The differencing schemes used are second-order accurate in both space and time. Both Schmidt and Lewis numbers are assumed to be unity. The inlet boundary conditions for $Re = 2000$ are summarized in Table 1. The Reynolds number is varied by changing the inflow velocities, but the velocity and momentum ratios remain constant. These velocities give an overall equivalence ratio of $\phi = 0.25$. Considering only the fuel and air injected into the cavity, the equivalence ratio is $\phi = 2.83$.

Table 1 Summary of inlet boundary conditions for $Re = 2000$

Location	Fluid	Temperature, K	Velocity, m/s
Channel	50% Air/50% combustion products	1000	5.164
Cavity	Heptane	300	0.081
Cavity	Air	300	1.54

The combustion is described as a one-step overall chemical reaction:

$$C_7H_{16} + 11(O_2 + 3.76N_2) \rightarrow 7CO_2 + 8H_2O + 41.36N_2 \tag{9}$$

and the chemical kinetics rate for the fuel is calculated from

$$\dot{\omega}_F = -A\rho^{a+b}Y_F^a Y_O^b e^{-E_a/R_uT} \tag{10}$$

in which the chemical rate constants $A = 1.2 \times 10^9$, $a = 0.25$, $b = 1.5$, and $E_a = 1.255 \times 10^8$ have been obtained from Westbrook and Dryer [30].

One parameter used to quantify the performance of different configurations is the combustion efficiency η_c. The combustion efficiency is a measure of how much of the fuel is consumed as a percentage of the amount injected. This fraction varies with time, and so it is integrated to give an overall efficiency:

$$\eta_c = \frac{\int_{t_0}^{t_0+T_c}\int \dot{\omega}_F \,\mathrm{d}V\,\mathrm{d}t}{\int_{t_0}^{t_0+T_c}\dot{m}_{F,\mathrm{in}}\,\mathrm{d}t} \tag{11}$$

in which $\dot{\omega}_F$ is the fuel reaction rate. This definition is used for combustion efficiency rather than the more commonly used definition using the fuel-mass flow in and out of the domain. Both are equivalent as $T \rightarrow \infty$, and a fully developed state occurs. However, the current definition converges to a stable solution more quickly than when considering only fuel at the boundaries. This behavior occurs because the current definition implicitly avoids the effect of the change in the amount of fuel stored in the computational domain on the efflux of fuel mass during the calculation. This effect is often significant during startup for cavity flows because there is a fill time. Flows over cavities are highly unsteady and oscillations can persist in the time integral of Eq. (11) for a prohibitively long time for numerical calculations. Where possible, the time evolution of Eq. (11) is presented rather than a single value for the combustion efficiency. The reader is then aware of any oscillations that may still be occurring in the value. Where a single representative value is given, it is the final time-averaged value at the termination of the calculation.

All computations include air injection into the cavity. Two different injection configurations have been considered, as shown in Fig. 1. The reinforcing configuration reinforces the natural rotation created by the main channel flow by injecting cold fuel high on the upstream wall and cold air low in the downstream wall. Conversely, the disrupting configuration injects the fuel low and the air high, disrupting the natural rotation. In both configurations, the air

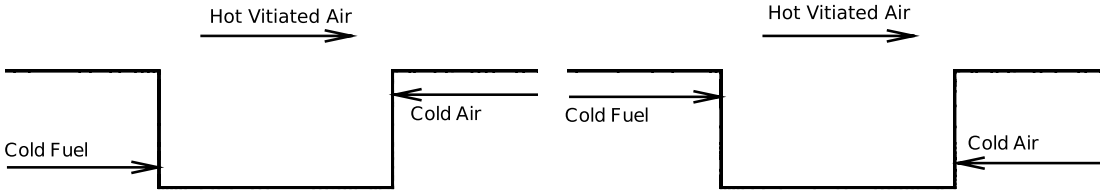

a) Disrupting **b) Reinforcing**

Fig. 1 Injection configurations.

injection is downstream of the fuel injection. The injection ports are square with a symmetry plane along their center. This allows the Cartesian coordinates to be retained, thus improving the accuracy of the calculation by eliminating any nonorthogonality in the mesh. The center-to-center spacing of the injection ports is three times the injector dimension. Details of the injection ports are shown in Fig. 2a, and the orientation of the axes is shown in Fig. 2b. The dimensions are given in terms of L, in which $L = 0.0025$ m. The dimensions in all figures are in SI units.

The overall combustion efficiency is influenced by the amount of mixing between the fuel and air, because the fuel and the oxidizer must mix before they can burn. Here, we define a mixedness parameter M locally as

$$M = 1 + \frac{(y_C - y_{C,p})(y_N - y_{N,p})}{\alpha^2} \tag{12}$$

in which y_m is a modified mass fraction of element m that considers only carbon and nitrogen atoms

$$y_m = \frac{Y_m}{Y_C + Y_N} \tag{13}$$

The perfectly mixed modified mass fraction $y_{m,p}$ is calculated from the mass flow rates of air and fuel injected into the cavity. A normalizing variable α is used to enforce a mixedness of zero if completely unmixed for either Y_N or Y_C approaching zero. It is given by

$$\alpha = \begin{cases} y_{C,p}, & (y_C - y_{C,p}) < 0 \\ y_{N,p}, & (y_C - y_{C,p}) > 0 \end{cases} \tag{14}$$

With complete mixing, a uniform mixture would yield a mixedness parameter of unity value.

Grid-dependence tests for a slot-injection case are shown in Fig. 3a. Here, X10 and X12 represent the number of grid points in each direction compared with a coarse grid, so that the X12 grid has 20% more grid points in each direction than the X10 grid. The difference in instantaneous combustion efficiency has a maximum of 3% and an average of less than 1%, indicating that the grid spacing is sufficiently fine. A comparison is made between various numerical approaches for the slot-injection case, in which fine-mesh 2-D calculations may be used. With slot injection, the constraints are 2-D, although some 3-D instabilities remain possible. So, it is interesting to compare both 2-D and 3-D calculations here. In addition, the periodic port injection is also compared in the figure. Because computational resources are limited, fewer total mesh points were used in the x and y directions for the 3-D mesh than for the 2-D simulations. The mesh points in 3-D were distributed so that they were more concentrated in regions where needed most: in the cavity and in the downstream boundary layer. The near-wall mesh spacing for the downstream boundary layer was kept consistent with the 2-D mesh, but fewer mesh points were used upstream of the cavity and in the upper half of the channel. Recall that slip is allowed on the upper channel wall, and so no boundary layer needs to be resolved. This redistribution of mesh points allows the calculations with 40 mesh points in the z direction. In an attempt to isolate the 3-D effects from the mesh effects, a 3-D simulation with completely 2-D boundary and initial conditions was calculated. This simulates a slot injection, and has identical boundary and initial conditions to the 2-D simulation. This case was repeated in 2-D using the exact mesh spacing as used in the 3-D calculation, so that any differences in the results come from the physical 3-D effects rather than any mesh effects. Here, 2-D with standard mesh and 3-D with discrete port injection are the simulations shown in Fig. 3a for the reinforcing injection. Plots of time-averaged combustion efficiencies are shown in Fig. 3b. The 2-D with 3-D mesh spacing and the 3-D with slot injection are the two additional cases described previously that use identical x and y mesh spacing. First of all, comparing the two 2-D results shows that there is some dependence on the mesh, and coarser meshes tend to give higher combustion efficiencies. The increase here is approximately 2.5%. When the same mesh spacing is used in 2-D and 3-D, the two lines are almost identical, indicating that 3-D effects are insignificant with 2-D boundary conditions at the given Reynolds number. The most significant increase occurs from the 3-D slot injection to the 3-D

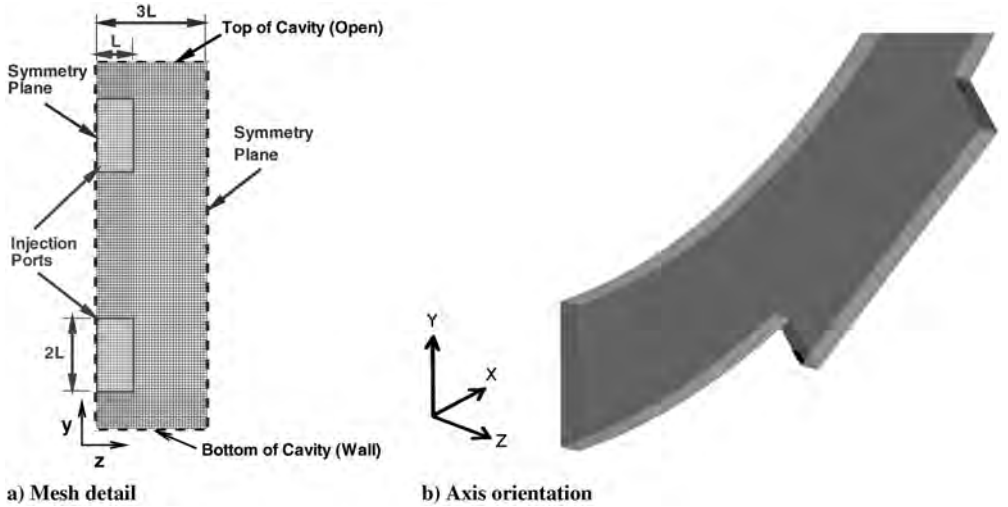

a) Mesh detail **b) Axis orientation**

Fig. 2 Cavity with disrupting injection.

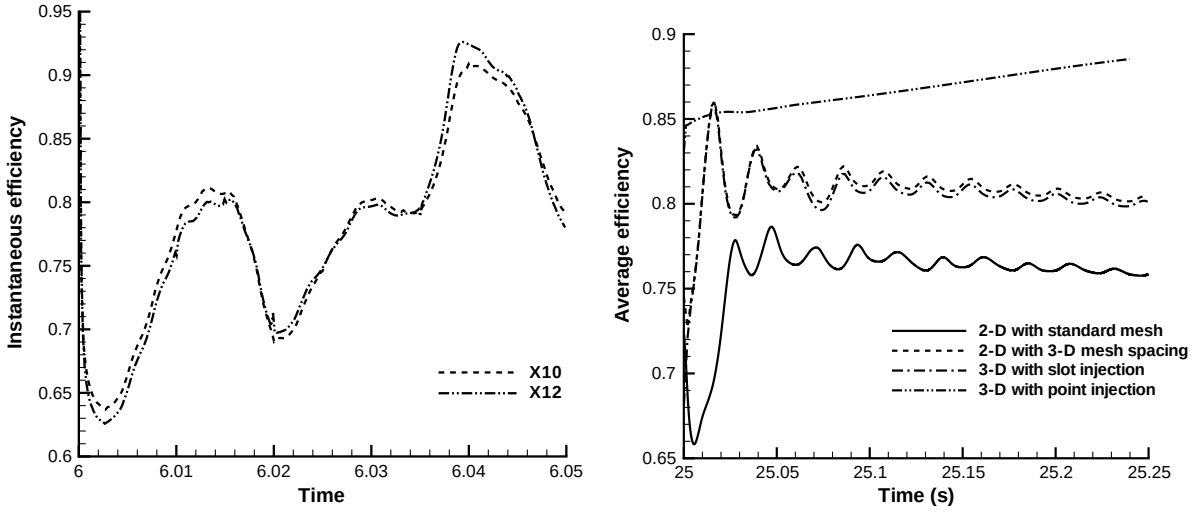

a) Instantaneous combustion efficiency b) Comparison of 2-D and 3-D combustion efficiencies

Fig. 3 Grid dependence; straight channel, reinforcing injection.

discrete port injection, which has 3-D boundary conditions. Here, the increase is 4–5%. We then conclude that, although there may be some grid-dependence effect in the observed improvements in combustion efficiencies, the increase is due primarily to the three dimensionality.

III. Results

A. Reacting Flow in Straight Channels

All of the reacting results presented here have a main channel-flow inlet temperature of 1000 K. The channel fluid is a vitiated mixture of 50% air and 50% combustion products. The temperature of the injected gaseous fuel or additional air is 300 K. The Reynolds number is based on the channel height and inlet flow properties. The channel height has been fixed at 0.05 m so that the Reynolds number varies with the inlet velocity. The cavity dimensions are denoted by $xxx \times yyy$, in which xxx and yyy are the length and depth of the cavity, respectively, as percentages of the channel height, so that the numbers give both the size and aspect ratio of the cavity. For example, 200×050 represents a cavity 0.1 m long and 0.025 m deep. The equivalence ratio ϕ represents the percentage of fuel compared to the overall stoichiometric conditions.

For a straight channel at $Re = 2000$, the combustion efficiencies for disrupting and reinforcing injection are 84.7 and 88.5%, respectively. The 3-D effects of the reinforcing and disrupting configurations differ significantly. Figure 4 shows the reaction-rate contours of a y-z planar slice 95% along the cavity length for the disrupting and reinforcing injections. The disrupting injection shows a significant three dimensionality with a circular region of high reaction rate. It is interesting that the region is circular despite the injection port being square. In contrast, the reinforcing injection shows very little three dimensionality, showing two 2-D sheets of high reaction rate. However, even for the disrupting-injection configuration, planar slices at other locations show that the 3-D effects are confined to a region close to the injection ports, the

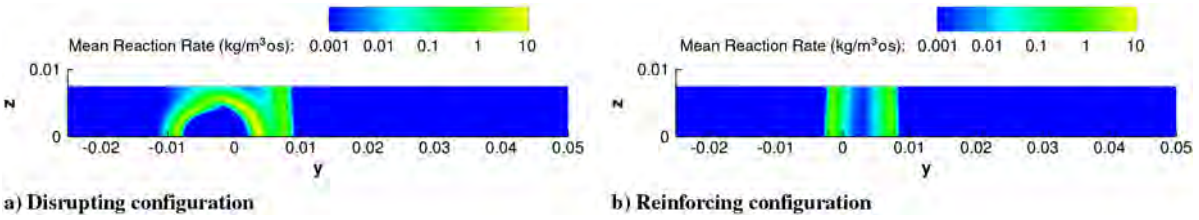

a) Disrupting configuration b) Reinforcing configuration

Fig. 4 Reaction-rate; slice 95% along cavity.

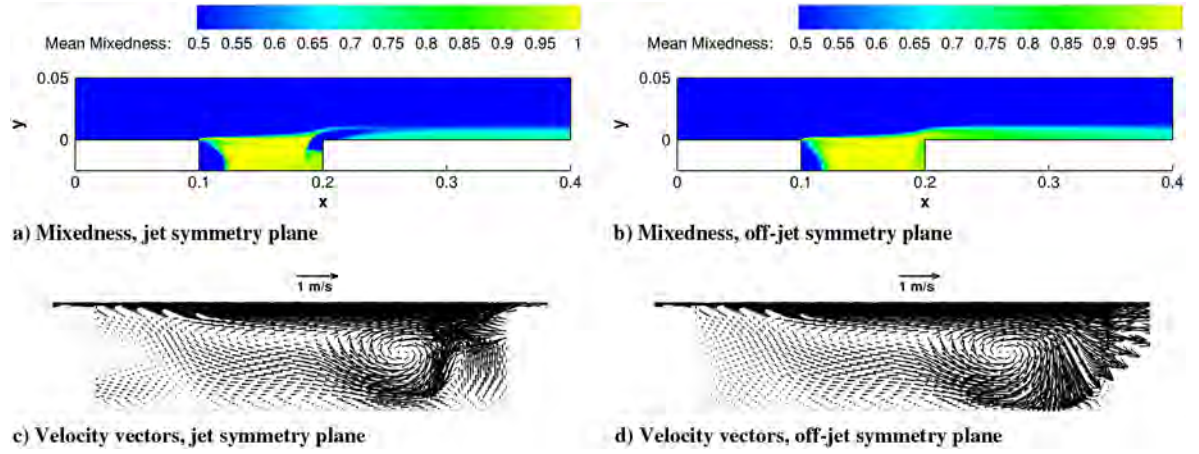

a) Mixedness, jet symmetry plane b) Mixedness, off-jet symmetry plane

c) Velocity vectors, jet symmetry plane d) Velocity vectors, off-jet symmetry plane

Fig. 5 Mean-mixedness and velocity vectors; disrupting injection.

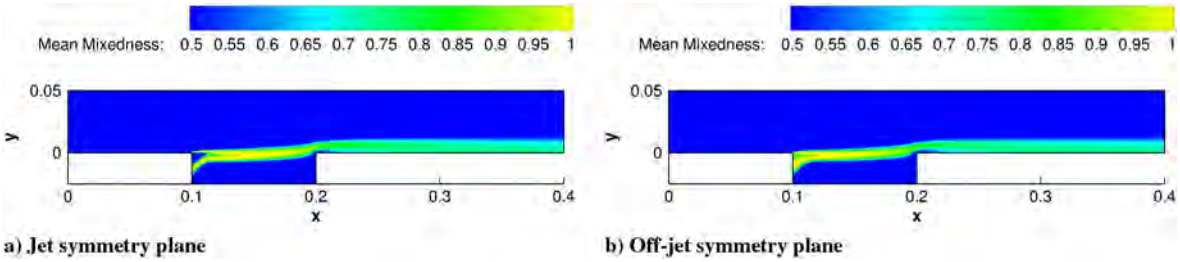

Fig. 6 Mean-mixedness; reinforcing injection.

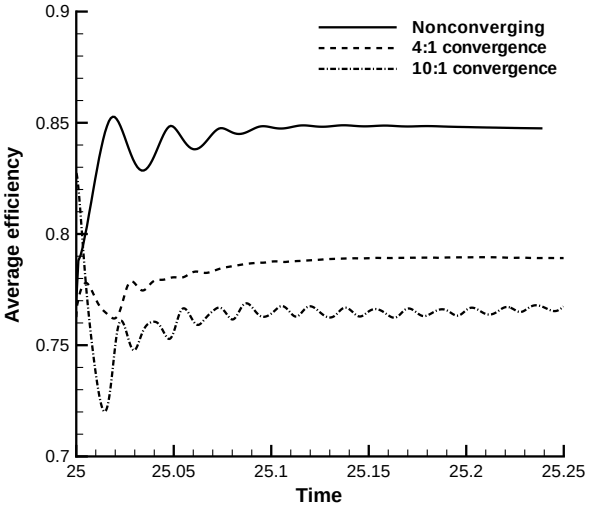

Fig. 7 Time-averaged combustion efficiencies; converging channels, disrupting injection.

only places where the boundary conditions introduce any three dimensionality.

Figure 5 shows the mean-mixedness contours for the disrupting configuration at the z-direction boundary planes. This shows that the fuel is very well mixed through most of the cavity and reasonably well mixed in the downstream boundary layer. Note that, because of the vitiated inflowing channel air, the freestream mixedness is not zero. The reinforcing configuration gives very different results, showing a thin region of high mixedness in the shear layer with a very low mixedness in the cavity, as seen in Fig. 6.

B. Reacting Flow in Converging Channels

Three area convergence ratios of 2:1, 4:1, and 10:1 are considered. Here, the ratio is between the channel height at the inlet and the channel height at the exit. All of the channels converge linearly. The exit Mach number is less than 0.1 for all convergence ratios.

Figure 7 shows the time-averaged combustion efficiencies of the simulations in nonconverging and converging channels with disrupting injection. Only the disrupting injection was considered here because it has shown greater 3-D effects in the previous simulations. The nonconverging channel has the highest efficiency, and the efficiency decreases as the convergence ratio increases. There are two main effects of increasing the channel velocity via channel convergence. First, the local Reynolds number over the cavity increases, which improves mixing. This by itself tends to improve the combustion efficiency. Second, the residence time in the channel decreases, which tends to decrease the combustion efficiency. The results show that the increase in mixing caused by a higher local Reynolds number in the cavity is not enough to overcome the reduced residence time caused by the acceleration. Recalling from Fig. 5 that the cavity mixedness for this case is already very high, this is not surprising.

C. Reacting Flow in Constant Area Turning Channels

The channel is turned through up to 90 deg, and the centerline arc length of the channel is kept at 0.4 m, the same as the straight-channel length. At $Re = 2000$ with a 90 deg turning angle, the centrifugal acceleration is 118 $\mathrm{m/s^2}$ or approximately 12 g, giving a nondimensional Froude number of $Fr = 2.13$, in which

$$Fr = \frac{U}{\sqrt{a_c l}} = \sqrt{\frac{R}{l}} \tag{15}$$

Here, R is the radius of curvature of the channel centerline. The radial location r, used hereafter, is defined as the distance from the center of the channel-centerline arc.

Figure 8 shows the combustion efficiencies for the cases with disrupting injection. The straight channel here shows a slightly higher combustion efficiency than the case with the cavity on the outside, and both give considerably higher efficiencies than the case with the cavity on the inside. The difference between the straight channel and

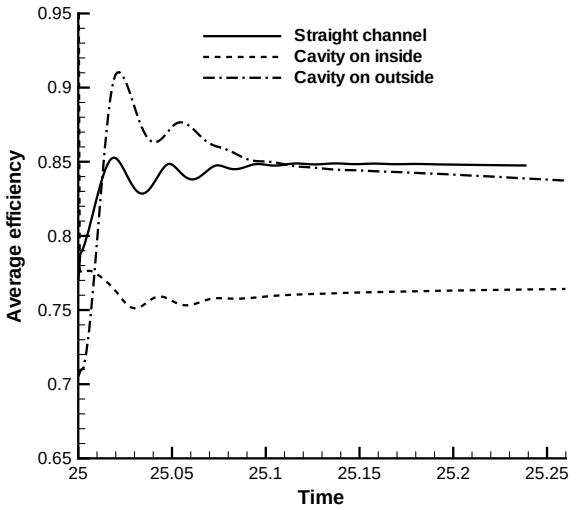

Fig. 8 Combustion efficiencies; turning channels, disrupting injection.

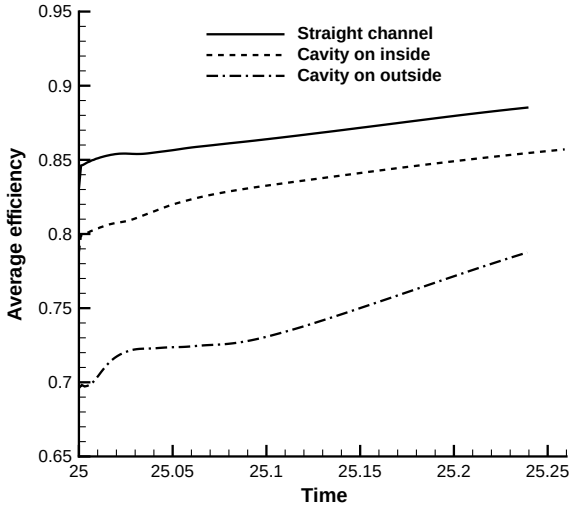

Fig. 9 Combustion efficiencies; turning channels, reinforcing injection.

the cavity on the outside is within the margin of error caused by the 3-D mesh and the method of calculating the combustion efficiency. It is, therefore, not conclusive as to which configuration has the higher efficiency.

The equivalent information for the reinforcing-injection configuration is shown in Fig. 9. Here, the case with the cavity on the outside has the lowest efficiency and the straight channel has the highest efficiency. The straight-channel results showed that the disrupting-injection configuration is more 3-D than the reinforcing injection. This is seen in Fig. 10, which shows the mean reaction rate in a slice at a location 95% along the length of the cavity. The disrupting injection exhibits a roughly circular region of high reaction rate, whereas the reinforcing injection shows only 2-D behavior in the form of planar flame sheets.

The velocity vectors at various r-z planes along the length of the channel are shown in Fig. 11 for the disrupting configuration with the cavity on the outside. Note that the scale of the velocity vectors in Fig. 11a is different from the other subfigures because the velocity in this plane is considerably higher. A vortex, which grows in strength with downstream distance, is evident near the outside curve. This vortex is similar to the vortex created by the Görtler instability that occurs with flow around a concave wall. This vortex does not appear, however, with the reinforcing injection and does occur to a lesser degree on the convex wall when the cavity is on the inside with the disrupting injection. It appears that the close proximity of the air injector to the cavity shear layer and channel flow causes this instability in the disrupting-injection case, and they are not true Görtler vortices, although the Görtler instability does strengthen the vortices when on the concave wall. These will be referred to as streamwise boundary-layer vortices. This lack of instability in the reinforcing case reduces the amount of mixing in the downstream boundary layer, and therefore the amount of reaction in the boundary layer. This has a larger detrimental effect on the case with the cavity on the outside, as seen in Fig. 9, because a greater proportion of the combustion occurs in the boundary layer due to the increased residence time.

Figure 12 shows the mean-mixedness contours in the jet symmetry plane for the disrupting- and reinforcing-injection configurations with the cavity on the outside. The mixedness contours show significant differences between the two injection configurations. With the disrupting injection, the mixedness is high throughout most of the cavity, whereas with the reinforcing injection, there is only a thin region of high mixedness in the boundary layer. The velocity vectors in Fig. 11 show that a vortex forms in the downstream half of the cavity for the disrupting injection, caused by the air injection interacting with the channel flow. This enhances mixing. With the reinforcing configuration, the air jet traverses most of the length of the cavity without being disrupted, causing very little mixing. Slices through other planes in the z direction are very similar for both injection configurations.

Similar results are seen with the cavity on the inside in Fig. 13. The high-mixedness region in the reinforcing-injection case is even smaller than with the cavity on the outside.

D. Reacting Flow in the Converging and Turning Channels

A more realistic representation of an actual turbine passage is a channel that turns and converges, creating acceleration in both the axial and transverse directions. Here, we consider channels turning through 90 deg with a 10:1 convergence ratio for the disrupting-injection configuration only. The combustion efficiencies for the cases with the cavity on the inside and the outside are compared with

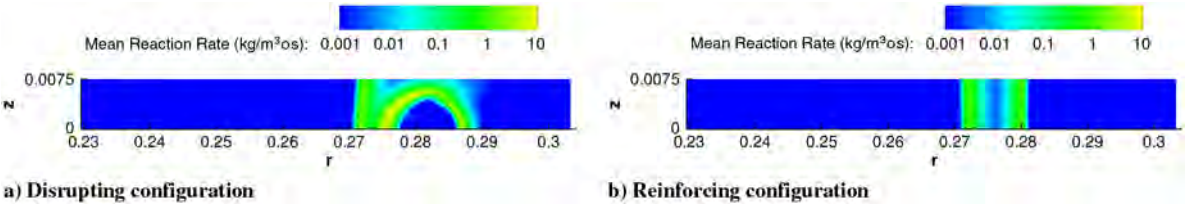

Fig. 10 Reaction-rate in plane 95% along outside cavity.

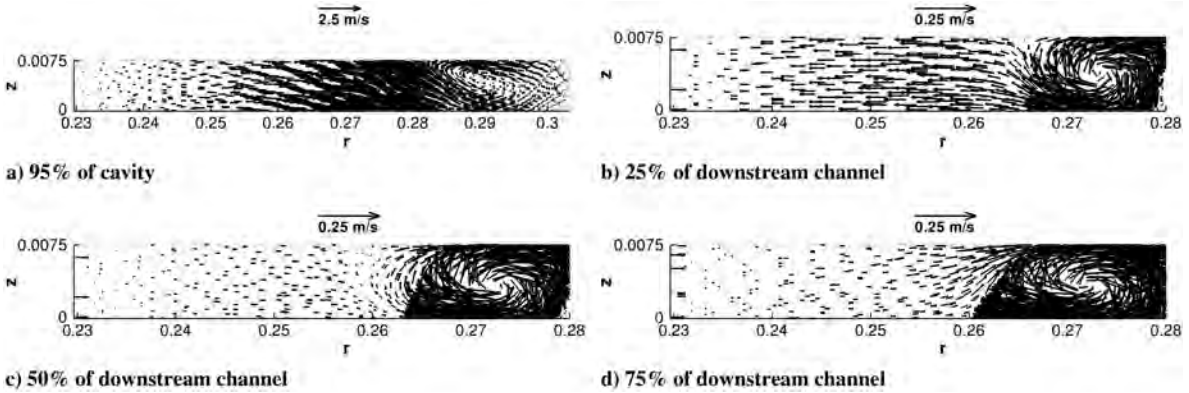

Fig. 11 Velocity vectors; outside cavity, disrupting injection.

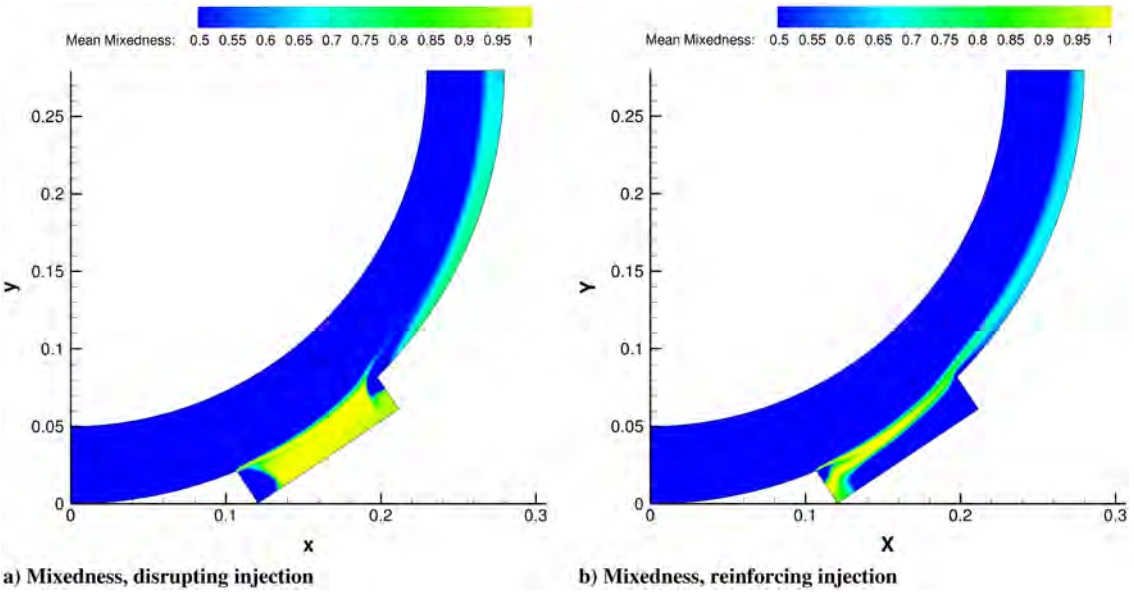

Fig. 12 Time-averaged mixedness; outside cavities.

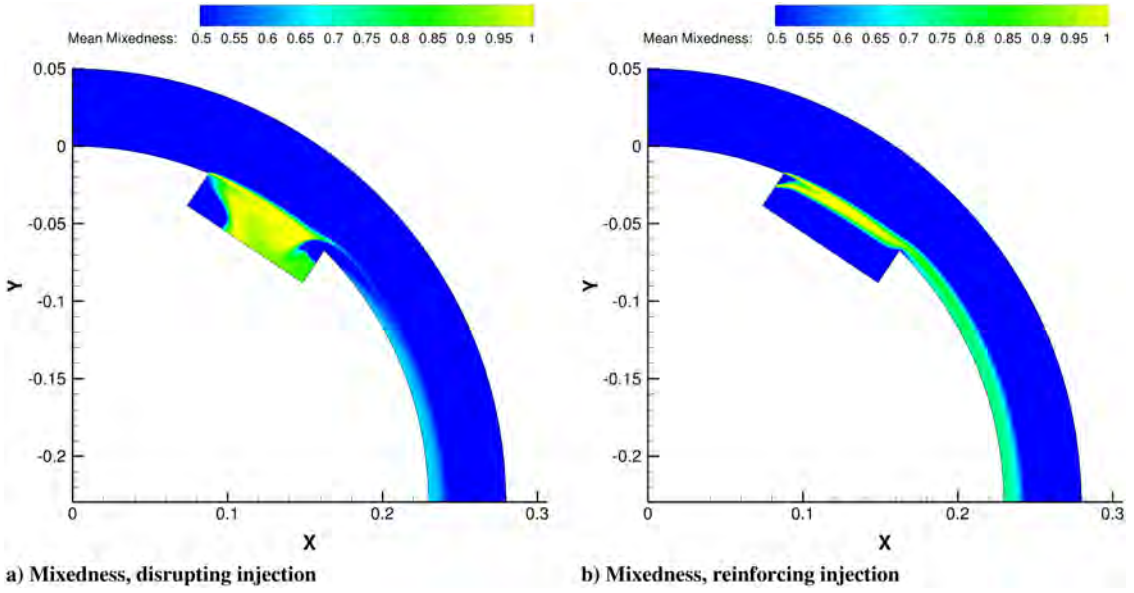

Fig. 13 Time-averaged mixedness; inside cavities.

the nonturning channel in Fig. 14. The cavity on the inside has the highest combustion efficiency and the cavity on the outside has the lowest.

Figure 15 shows the time-averaged mixedness contours for the 3-D converging and turning cases. The case with the cavity on the outside has the main channel flow penetrating into the cavity. The mixedness contours with the cavity on the outside are similar to the mixedness contours in the top half of the cavity on the inside. The case with the cavity on the outside loses a portion of the cavity as a low-speed zone for mixing.

A summary of all of the combustion efficiencies is shown in Fig. 16 and in Table 2. Efficiencies at the end of the calculation are given. The trend with a turning angle, as shown in Fig. 16a, is unclear for the nonconverging cases, but there is a clear improvement in combustion efficiency from outside to inside for the converging-channel case. Figure 16b shows two clear trends. First, the combustion efficiency decreases as the channel convergence increases. Second, the effect of the cavity location is much more significant with the channel convergence.

Table 2 summarizes all of the combustion efficiencies calculated for the 3-D geometry. The channel convergence decreases the combustion efficiency in all cases, except for the case with the cavity

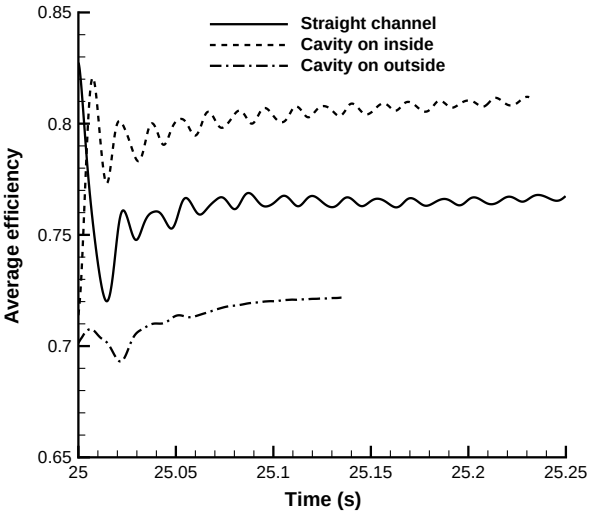

Fig. 14 Time-averaged combustion efficiencies; 10:1 converging channels.

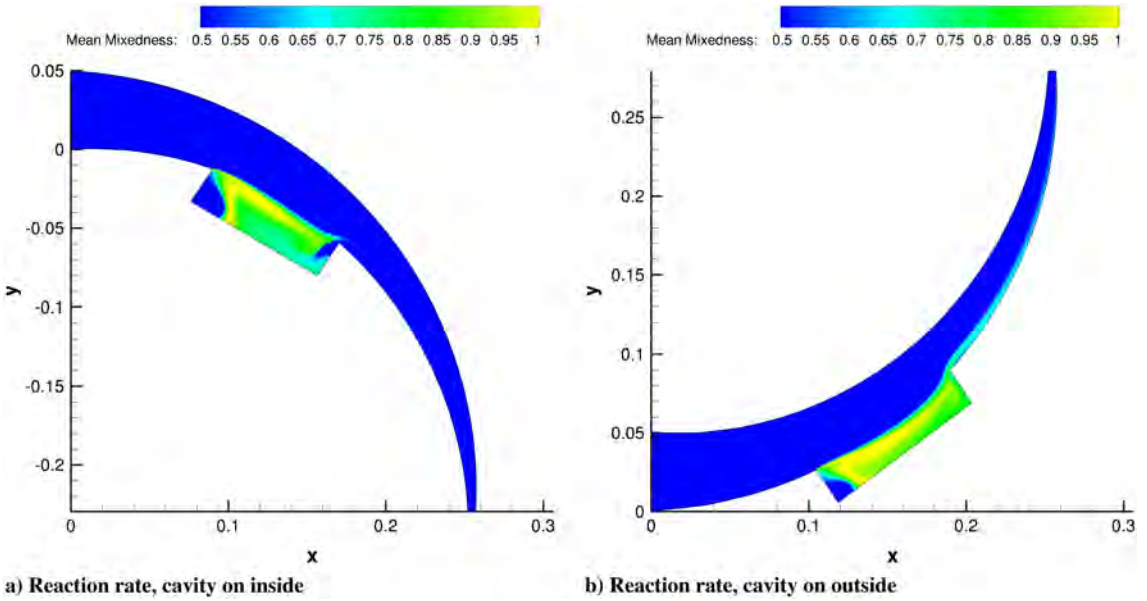

a) Reaction rate, cavity on inside b) Reaction rate, cavity on outside

Fig. 15 Time-averaged mixedness; converging and turning channels, disrupting injection.

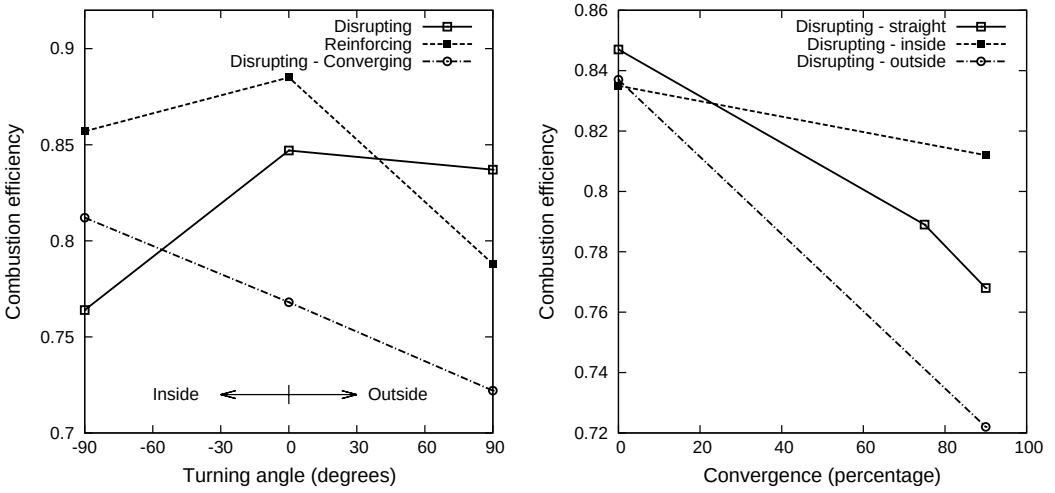

a) Combustion efficiency vs turning angle b) Combustion efficiency vs convergence ratio

Fig. 16 Summary of combustion efficiencies.

on the inside of a turning channel. The nonconverging channel with the cavity on the inside performs poorly compared to other configurations. However, the same cavity location in a converging channel causes the combustion efficiency to increase by about 5%. For the case with the cavity on the outside of the channel, the efficiency dropped more than 10% due to convergence. This increase with convergence when the cavity is on the inside is due to two factors. First, the channel convergence increases the local Reynolds number and turbulent mixing regardless of the location of the curvature or cavity location. Second, when the cavity is on the inside, the higher-speed channel flow curves out from the cavity, essentially increasing the size of the low-speed mixing region.

Table 2 Summary of combustion efficiencies for all 3-D calculations[a]

Curvature	Convergence	Disrupting	Reinforcing
— —	— —	0.847	0.885
90 deg inside	— —	0.764	0.857
90 deg outside	— —	0.837	0.788
— —	4:1	0.789	— —
— —	10:1	0.768	— —
90 deg inside	10:1	0.812	— —
90 deg outside	10:1	0.722	— —

[a]$Re = 2000$

IV. Conclusions

The authors have addressed important aspects for cavity combustion relevant to mixing and burning in the turbine stators that have not been addressed previously: effects of converging channels; effects of turning channels; effects of disrupting injection vs other types; and roles of the Rayleigh–Taylor, Rayleigh centrifugal, and Görtler instabilities in these cavity-channel-coupled flows. A three-dimensional (3-D) unsteady direct numerical simulation of the multicomponent reacting Navier–Stokes system of equations has been performed with various air- and fuel-injection configurations, and consideration of different cavity-channel configurations.

Useful combustion efficiency and mixedness parameters for this unsteady reacting flow have been formulated and calculated.

The injection locations of fuel and air can have significant impacts on the flowfield and on the combustion efficiency. Disrupting air injection close to the downstream shear layer can cause 3-D instabilities that improve the combustion efficiency. Streamwise

boundary-layer vortices appear only with the disrupting configuration. The effect of the injection location on combustion efficiency is greater for converging channels.

The combustion efficiency decreases as the convergence ratio increases for all injection configurations and cavity locations. Because the cavity is already well mixed, the combustion efficiency decreases with flow acceleration because of the decreased residence time.

Acknowledgments

The authors wish to thank the U.S. Air Force Office of Scientific Research for supporting this research through grant FA 9550-06-1-0194 with Julian Tishkoff as the scientific officer. W. Mel Roquemore and Joseph Zelina of the U.S. Air Force Research Laboratory are also thanked for their helpful advice.

References

[1] Sirignano, W. A., and Liu, F., "Performance Increases for Gas-Turbine Engines Through Combustion Inside the Turbine," *Journal of Propulsion and Power*, Vol. 15, No. 1, 1999, pp. 111–118. doi:10.2514/2.5398

[2] Sirignano, W. A., Dunn-Rankin, D., Liu, F., Colcord, B. J., and Puranam, S. V., "Turbine Burners: Performance Improvement and Challenge of Flameholding," *AIAA Journal*, Vol. 50, No. 8, 2012, pp. 1645–1669. doi:10.2514/1.J051562

[3] Liu, F., and Sirignano, W. A., "Turbojet and Turbofan Engine Performance Increases Through Turbine Burners," *Journal of Propulsion and Power*, Vol. 17, No. 3, 2001, pp. 695–705. doi:10.2514/2.5797

[4] Hsu, K.-Y., Goss, L. P., and Trump, D. D., "Performance of a Trapped-Vortex Combustor," AIAA Paper 95-0810, Jan. 1995.

[5] Hsu, K.-Y., Goss, L. P., and Roquemore, W. M., "Characteristics of a Trapped-Vortex Combustor," *Journal of Propulsion and Power*, Vol. 14, No. 1, 1998, pp. 57–65. doi:10.2514/2.5266

[6] Katta, V. R., and Roquemore, W. M., "Numerical Studies on Trapped-Vortex Concepts for Stable Combustion," *Journal of Engineering for Gas Turbines and Power*, Vol. 120, No. 1, 1998, pp. 60–68. doi:10.1115/1.2818088

[7] Katta, V. R., and Roquemore, W. M., "Study on Trapped-Vortex Combustor—Effect of Injection on Flow Dynamics," *Journal of Propulsion and Power*, Vol. 14, No. 3, 1998, pp. 273–281. doi:10.2514/2.5286

[8] Mathur, T., Gruber, M., Jackson, K., Donbar, J., Donaldson, W., Jackson, T., and Billig, F., "Supersonic Combustion Experiments with a Cavity-Based Fuel Injector," *Journal of Propulsion and Power*, Vol. 17, No. 6, 2001, pp. 1305–1312. doi:10.2514/2.5879

[9] Davis, D. L., and Bowersox, R. D. W., "Stirred Reactor Analysis of Cavity Flame Holders for Scramjets," AIAA Paper 97-3274, July 1997.

[10] Davis, D. L., and Bowersox, R. D. W., "Computational Fluid Dynamics Analysis of Cavity Flame Holders for Scramjets," *Thirty-Third AIAA Joint Propulsion Conference*, Seattle, WA, AIAA Paper 97-3270, July 1997.

[11] Yu, K., Li, J. G., Chang, X. Y., Chen, L. H., and Sung, C. J., "Investigation of Kerosene Combustion Characteristics with Pilot Hydrogen in Model Supersonic Combustors," *Journal of Propulsion and Power*, Vol. 17, No. 6, 2001, pp. 1263–1271. doi:10.2514/2.5874

[12] Yu, K., Wilson, K. J., Smith, R. A., and Schadow, K. C., "Experimental Investigation on Dual-Purpose Cavity in Supersonic Reacting Flows," AIAA Paper 98-0723, Jan. 1998.

[13] Yu, K., Li, J. G., Chang, X. Y., Chen, L. H., and Sung, C. J., "Investigation of Fuel Injection and Flame Stabilization in Liquid Hydrocarbon-Fueled Supersonic Combustors," AIAA Paper 01-3608, July 2001.

[14] Yu, K., Wilson, K. J., and Schadow, K. C., "Effect of Flame-Holding Cavities on Supersonic-Combustion Performance," *Journal of Propulsion and Power*, Vol. 17, No. 6, 2001, pp. 1287–1295. doi:10.2514/2.5877

[15] Yu, K., Li, J. G., Chang, X. Y., Chen, L. H., and Sung, C. J., "Fuel Injection and Flame Stabilization in a Liquid-Kerosene-Fueled Supersonic Combustor," *Journal of Propulsion and Power*, Vol. 19, No. 5, 2003, pp. 885–893. doi:10.2514/2.6179

[16] Kim, K. M., Baek, S. W., and Han, C. Y., "Numerical Study on Supersonic Combustion with Cavity-Based Fuel Injection," *International Journal of Heat and Mass Transfer*, Vol. 47, No. 2, 2004, pp. 271–286. doi:10.1016/j.ijheatmasstransfer.2003.07.004

[17] Rasmussen, C. C., Driscoll, J. F., Hsu, K.-Y., Donbar, J. M., Gruber, M. R., and Carter, C. D., "Stability Limits of Cavity-Stabilized Flames in Supersonic Flow," *Proceedings of the Combustion Institute*, Vol. 30, No. 2, 2005, pp. 2825–2833. doi:10.1016/j.proci.2004.08.185

[18] Puranam, S. V., Arici, J., Sarzi-Amade, N., Dunn-Rankin, D., and Sirignano, W. A., "Turbulent Combustion in a Curving, Contracting Channel with a Cavity Stabilized Flame," *Proceedings of the Combustion Institute*, Vol. 32, No. 2, 2009, pp. 2973–2981. doi:10.1016/j.proci.2008.06.161

[19] Sirignano, W. A., and Kim, I., "Diffusion Flame in a Two-Dimensional, Accelerating Mixing Layer," *Physics of Fluids*, Vol. 9, No. 9, 1997, pp. 2617–2630. doi:10.1063/1.869378

[20] Fang, X., Liu, F., and Sirignano, W. A., "Ignition and Flame Studies for an Accelerating Transonic Mixing Layer," *Journal of Propulsion and Power*, Vol. 17, No. 5, 2001, pp. 1058–1066. doi:10.2514/2.5844

[21] Mehring, C., Liu, F., and Sirignano, W. A., "Ignition and Flame Studies for an Accelerating Transonic Turbulent Mixing Layer," AIAA Paper 01-0190, Jan. 2001.

[22] Cai, J., Icoz, O., Liu, F., and Sirignano, W. A., "Ignition and Flame Studies for an Accelerating Transonic Mixing Layer in a Curved Duct Flow," AIAA Paper 01-0180, Jan. 2001.

[23] Cheng, F., Liu, F., and Sirignano, W. A., "Nonpremixed Combustion in an Accelerating Transonic Flow Undergoing Transition," *AIAA Journal*, Vol. 45, No. 12, 2007, pp. 2935–2946. doi:10.2514/1.31146

[24] Cheng, F., Liu, F., and Sirignano, W. A., "Nonpremixed Combustion in an Accelerating Turning Transonic Flow Undergoing Transition," *AIAA Journal*, Vol. 46, No. 5, 2008, pp. 1204–1215. doi:10.2514/1.35209

[25] Cheng, F., Liu, F., and Sirignano, W. A., "Reacting Mixing-Layer Computations in a Simulated Turbine-Stator Passage," *Journal of Propulsion and Power*, Vol. 25, No. 2, 2009, pp. 322–334. doi:10.2514/1.37739

[26] Drazin, P. G., and Reid, W. H., *Hydrodynamic Stability*, 2nd ed., Cambridge Univ. Press, Cambridge, England, U.K., 2004, pp. 116–120.

[27] Colcord, B. J., Sirignano, W. A., and Liu, F., "Flameholding in Converging and Turning Channels over Cavities with Slot Injection," *Combustion Science and Technology*, 2013 (in press).

[28] OpenFOAM, Software Package, Ver. 1.6.x, OpenCFD, Bracknell, England, U.K., 2004, http://www.openfoam.com [retrieved 22 June 2010].

[29] Sweby, P. K., "High Resolution Schemes Using Flux-Limiters for Hyperbolic Conservation Laws," *SIAM Journal on Numerical Analysis*, Vol. 21, No. 5, 1984, pp. 995–1011. doi:10.1137/0721062

[30] Westbrook, C. K., and Dryer, F. L., "Simplified Reaction Mechanisms for the Oxidation of Hydrocarbon Fuels in Flames," *Combustion Science and Technology*, Vol. 27, Nos. 1–2, 1981, pp. 31–43. doi:10.1080/00102208108946970

E. Gutmark
Associate Editor